Supplemental material: Superradiance for atoms trapped along a photonic crystal waveguide

A. Goban[1,2,†], C.-L. Hung[1,2,†,‡], J. D. Hood[1,2,†], S.-P. Yu[1,2,†],
J. A. Muniz[1,2], O. Painter[2,3], and H. J. Kimble[1,2,*]
[1] *Norman Bridge Laboratory of Physics 12-33*
[2] *Institute for Quantum Information and Matter, California Institute of Technology, Pasadena, CA 91125, USA and*
[3] *Thomas J. Watson, Sr., Laboratory of Applied Physics 128-95*
(Dated: July 11, 2015)

We provide supporting information for our manuscript [1], including device characterization, finite different time domain (FDTD) calculations for collective coupling rates, lifetime of trapped atoms along the APCW, and model for superradiance of trapped atoms.

I. DEVICE CHARACTERIZATION

A schematic of the alligator photonic crystal waveguide (APCW) is illustrated in Fig. SM1(a). The waveguide is made from 200-nm thick stoichiometric SiN with refractive index $n = 2.0$ [2]. The APCW is formed by two parallel SiN nanobeams separated by 238 nm with periodic corrugations at the outer edges (Fig. SM1). The dimensions of the nominal photonic crystals are the following: lattice constant $a = 371$ nm, gap $g = 238$ nm, width $w = 157$ nm, and tooth amplitude $A = 131$ nm, as shown in Fig. SM1(b). The nominal photonic crystal section consists of $N_{\rm cell} = 150$ unit cells (length $L \simeq 55.7\mu$m), terminated by 30 tapered cells on each side to provide 'mode-matching' to and from double nanobeams sections. Photons can be coupled into and out of the APCW from conventional cleaved-fibers at either end of the structure.

The APCW is characterized by measuring the transmission spectrum $T_0(\nu)$ without atoms. The resonant structure around frequencies ν_i displayed in Fig. SM2 arises from reflections in the tapered sections at the two ends of the APCW. The free spectral range $\Delta\nu_i = \nu_{i+1} - \nu_i$ between resonances decreases as the band edge frequency $\nu_{\rm BE}$ is approached, which is a signature of an increasing group n_g index near $\nu_{\rm BE}$, with $n_g \propto 1/\Delta\nu_i$ for an ideal structure. The distance from the band edge frequency $\nu_{\rm BE}$ to the first resonance ν_1 is about 6 part in 10^4, resulting in a group index $n_g \sim 11$; see discussion below and Fig. SM2.

Our experiment in Ref. [1] is operated around the frequency ν_A of the D_1: $6S_{1/2},\ F = 3 \rightarrow 6P_{1/2},\ F' = 4$ transition in atomic Cs, with ν_1 aligned near ν_A by controlling fabrication accuracy at a level of 10^{-3}. Fine tuning for $\nu_1 = \nu_A$ to 3ppm accuracy is achieved by way of a guided-mode (GM) heating beam with a wavelength of 850 nm and optimum power, typically $P \geq 100\mu$W. In addition, we turn on a strong GM heating beam for 100 ms at the end of each experimental cycle in order to keep the device clean by desorbing Cs from the APCW.

In order to estimate the group index n_g, single-taper reflectivity R_t, and intensity loss $e^{-2\zeta}$, we use a model based on the transfer matrix formalism for a periodic system to fit the transmission spectrum [3], which we now briefly describe. The

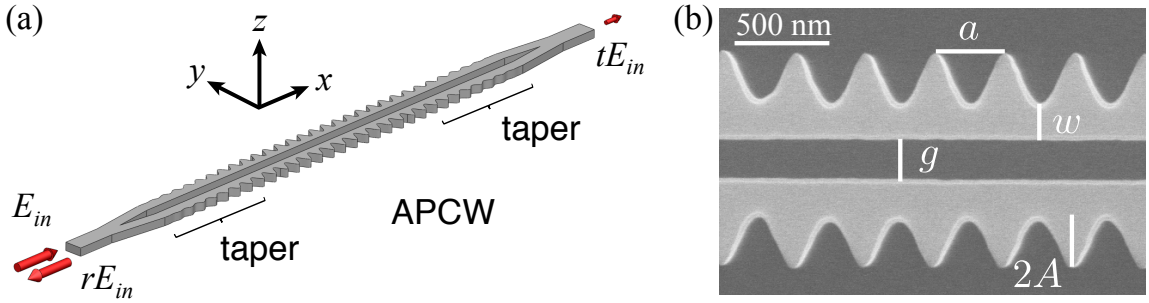

FIG. SM1: (a) Schematic of the APCW. An incident field $E_{\rm in}$ excites the TE-like fundamental mode, and the intensities for the transmitted $tE_{\rm in}$ and reflected field $rE_{\rm in}$ are recorded for device characterization. (b) SEM image of APCW with lattice constant a, gap g, width w, and tooth amplitude A.

[†] These authors contributed equally to this research.
[‡] Present address: Purdue University, West Lafayette, IN 47907, USA
[*] Correspondence and requests for materials should be addressed to HJK (hjkimble@caltech.edu.)

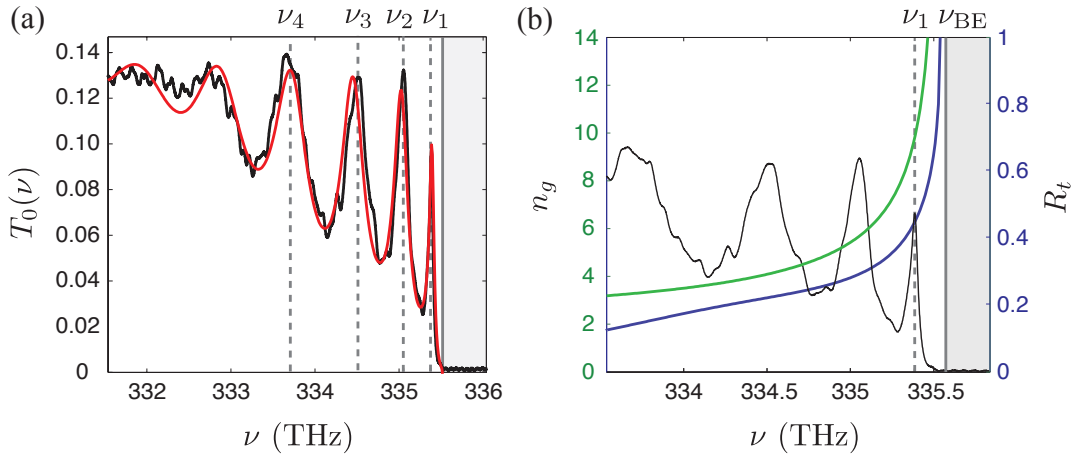

FIG. SM2: (a) Measured transmission spectrum $T_0(\nu)$ for the APCW (black) around the edge of the dielectric band and the model fit (red). The dashed lines mark the resonant frequencies ν_i from reflections in the taper sections and the solid line marks the band edge frequency $\nu_{\rm BE}$. (b) Estimated group index n_g (green) and taper reflection R_t (blue) from the fitted model. For the reference, the transmission spectrum $T_0(\nu)$ is overlaid. At the first resonance ν_1 marked by the dashed line, the group index is $n_g \approx 11$, and the taper reflection is $R_t \approx 0.48$.

dispersion relation for the wavevector $k(\nu)$ near the band edge is approximated by the fitting function [3],

$$k(\nu) = k_0 \left(1 - \sqrt{\frac{(\nu_0 - \nu(1+i\kappa))^2 - \Delta_g^2}{\nu_{\rm F}^2 - \Delta_g^2}} \right), \tag{1}$$

where the wavevector at the band edge is $k_0 = \pi/a$. Here, fitting parameters are the frequency at the center of the band gap ν_0, the size of the band gap $2\Delta_g$, the asymptotic group velocity far from the band edge $2\pi\nu_{\rm F}/k_0$, and the loss parameter κ. The loss parameter κ comes from using perturbation theory to add a small imaginary component to the dielectric constant of the material, resulting in an imaginary propagation constant that is approximately given by

$$\mathrm{Im}[k(\nu)] \approx \frac{2\pi\nu}{v_{\rm g}}\kappa. \tag{2}$$

It provides a convenient way to model losses that scale with inverse group velocity.

Next we consider the weak cavity formed by the taper reflections R_t. The single-pass phase accumulation ϕ and single-pass power transmission $e^{-2\zeta}$ through the cavity are written by

$$\phi = N_{\rm cell} a\, \mathrm{Re}[k] \quad \text{and} \quad \zeta = N_{\rm cell} a\, \mathrm{Im}[k], \tag{3}$$

where $N_{\rm cell}$ is the number of unit cells of the APCW and a is the lattice constant. Then, the transmission through a symmetric cavity with mirrors R_t is given by

$$T_{\rm cavity} = \frac{1}{1 + \mathcal{L} + F \sin^2[\phi]}, \tag{4}$$

where the coefficient F and loss coefficient $\mathcal{L}$ are given by

$$\mathcal{L} = \frac{\left(1 - R_t\, e^{-2\zeta}\right)^2}{e^{-2\zeta}\,(1-R_t)^2} - 1 \quad \text{and} \quad F = \frac{4R_t}{(1-R_t)^2}. \tag{5}$$

In order to fit this model to the measured transmission spectrum, first we use the dispersion model (Eq. (1) with $\kappa = 0$) to fit the positions of the cavity resonances to. Second, we fit Eq. (4) with no loss ($\mathcal{L} = 0$) to the transmitted spectrum by using the fitted dispersion model to find ϕ and by using a fitting function for F [3], namely

$$(F)^{-1/2} = A_1(\mathrm{d}\nu/\Delta_g) + A_2(\mathrm{d}\nu/\Delta_g)^2 + A_3(\mathrm{d}\nu/\Delta_g)^3, \tag{6}$$

where $d\nu$ is the distance in frequency from the band edge. Finally, we find the loss parameter ζ that makes the on-resonant peak heights of the model best match our measurement.

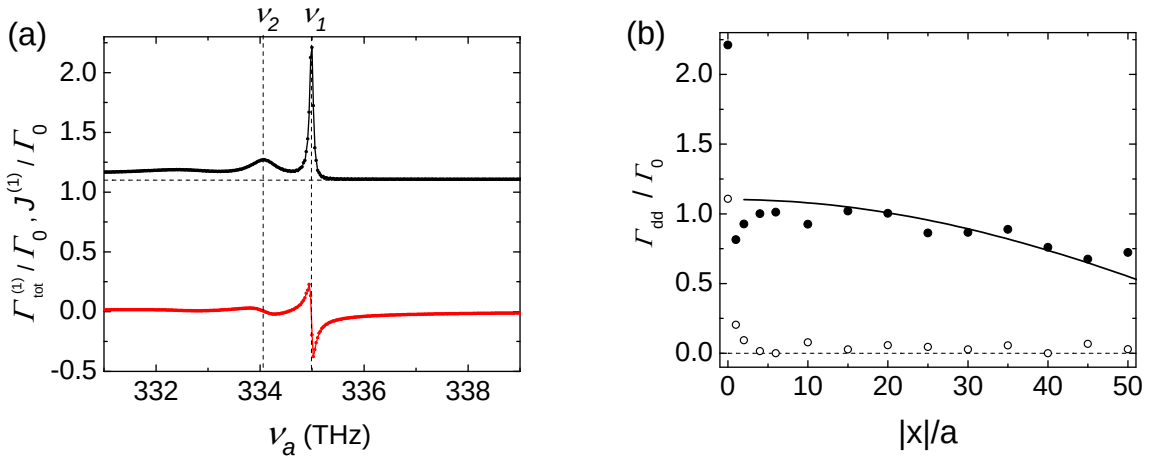

FIG. SM3: (a) Single-atom decay rate $\Gamma^{(1)}_{\rm tot}$ (black circles) and excited state level shift $J^{(1)}$ (red circles) at $\mathbf{r}_a = (0, 0, z_1)$ nm. Vertical dashed lines mark the frequencies of the first two guided mode resonances, ν_1 and ν_2, near the band gap (frequency range $\nu_a \gtrsim \nu_{\rm BE} = 335.1$ THz where $\Gamma_{\rm tot}$ appears constant) that are supported by the finite length of the APCW. Horizontal dashed line indicates $\Gamma'/\Gamma_0 = 1.1$, estimated from the constant $\Gamma^{(1)}_{\rm tot}$ in the band gap region. (b) Dissipative coupling rate $\Gamma_{\rm dd}(x) \equiv |\Gamma(\mathbf{r}_a, \mathbf{r}_a + x\hat{\mathbf{x}})|$ between two trapped atoms separated by x, with their resonant frequencies at either $\nu_a = \nu_1$ (solid circles) or $\nu_a = 336$ THz $> \nu_{\rm BE}$ inside the band gap (open circles), respectively. Solid line is an analytical calculation considering actual finite size of the APCW (Fig. SM1).

Figure SM2 (a) shows the measured transmission spectrum (black curve), overlaid with the model fit (red curve). The fitted parameters for the dispersion model are $2\Delta_g$ = 14.44 THz, $\nu_{\rm F}/\nu_0$ = 0.60, and ν_0 = 342.8 THz. The fitted parameters for F are A_1 = 9, A_2 =-48, and A_3 = 128. The fitted loss parameter is $\kappa = 1.5 \times 10^{-5}$. At the first resonance ν_1, the model linewidth is 55 GHz, in reasonable agreement with the measured linewidth of 66 GHz. The fitted dispersion relation is used to estimate the group index, and the fitted cavity model is used to estimate R_t and the single pass transmission $e^{-2\zeta}$, as shown in Fig. SM2 (b). At the first resonance, the group index is $n_g \approx 11$, the taper reflection is $R_t \approx 0.48$ and the single-pass transmission is $e^{-2\zeta} \approx 0.89$ [3], resulting in a peak intensity enhancement $\mathcal{E}_I \approx 4.1$. Since the propagation loss in the APCW is reasonably small, we ignore the loss in our analysis in the following sections.

We note that the principal contribution to the enhanced decay rate for an atom coupled to the APCW is the enhancement $n_g \approx 11$ from a reduced group velocity for operation near the band edge. The "parasitic cavity" enhancement is estimated to be a factor of $\mathcal{E}_I \approx 4.1 < n_g$. Moreover, our ability to excite Dicke superradiance benefits directly from the standing wave-like electric field of the guide mode near the band edge $\nu_{\rm BE}$. Unlike conventional high-finess cavity, the parasitic cavity plays a minor role in the observed superradiance and does not provide a standing-wave like coupling rate $\Gamma_{\rm 1D}\cos^2(kx)$ as in our experiment near the bandedge of the APCW; without operating near the band edge, superradiant effect becomes less significant due to uncontrolled optical phases seen by atoms randomly distributed along the APCW.

For the APCW reported in [1], cesium hyperfine splitting 9.2GHz is small compared to the linewidth (FWHM 66GHz) of the first resonance as well as its detuning from the band edge $\nu_{\rm BE} - \nu_1 \sim 200$ GHz. When aligning ν_1 to $6P_{1/2}, F = 4 \rightarrow 6S_{1/2}, F = 3$ transition frequency. Both decay rates into $F = 3$ and $F = 4$ hyperfine ground states should be similarly enhanced by factors that differ no more than 10%.

II. FINITE DIFFERENT TIME DOMAIN CALCULATIONS FOR COLLECTIVE COUPLING RATES

Due to strong coupling to the TE-like GM in the APCW, trapped atoms experience both enhanced atomic decay rates as well as collective Lamb shifts. To estimate the size of these effects, we perform FDTD calculations and Fourier analysis as described in Ref. [4] to obtain the two-point Green's tensor $\mathbf{G}(\mathbf{r}_1, \mathbf{r}_2, \omega)$ for the APCW shown in Fig. SM1. We then evaluate dissipative and coherent coupling rates, respectively, as [5–7]

$$\Gamma(\mathbf{r}_1, \mathbf{r}_2) = \frac{2\mu_0\omega_a^2}{\hbar}\mathbf{d}\cdot{\rm Im}[\mathbf{G}(\mathbf{r}_1, \mathbf{r}_2, \omega_a)]\cdot\mathbf{d} \quad (7)$$

$$J(\mathbf{r}_1, \mathbf{r}_2) = -\frac{\mu_0\omega_a^2}{\hbar}\mathbf{d}\cdot{\rm Re}[\mathbf{G}_{sc}(\mathbf{r}_1, \mathbf{r}_2, \omega_a)]\cdot\mathbf{d}, \quad (8)$$

where $\mathbf{d}$ is the transition dipole moment, ω_a the transition frequency, μ_0 the vacuum permeability, and $\hbar$ Planck's constant divided by 2π. Here, $\mathbf{G}_{sc} = \mathbf{G} - \mathbf{G}_0$ is the scattering Green's tensor, in which the vacuum contribution $\mathbf{G}_0$ is subtracted from

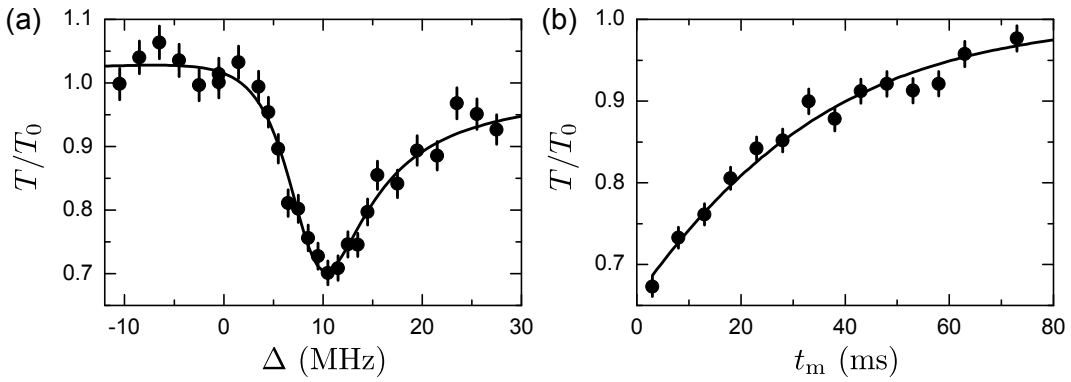

FIG. SM4: (a) Normlaized transmission spectrum. Each point in the spectrum is an average over 10 experiment repetitions. Black curve shows the fit to Eq. (9) at $t_{\rm m} = 2.5$ ms with $\theta = -0.6 \pm 0.1$, $C_0 = 0.24 \pm 0.1$, $\Gamma = 8.2 \pm 0.6$ MHz and $\Delta_0 = 9.3 \pm 0.3$ MHz. (b) Normalized transmission T/T_0 as a function of the holding time, measured by the on resonant guided-mode probe with $\Delta = 10.5$ MHz. By fitting the measured data to Eq. (9) with fitted parameters extracted in Fig. SM4 (a), we obtain the lifetime of $\tau_{\rm GM} = 28 \pm 2$ ms (black curve).

the total Green's tensor $\mathbf{G}$; $\mathrm{Im}[.]$ and $\mathrm{Re}[.]$ represent imaginary and real parts, respectively. The coupling rate $\tilde{\Gamma} = \Gamma/2 + iJ$ controls collective excitation dynamics of trapped atoms along the APCW.

We obtain single-atom rates by setting $\mathbf{r}_1 = \mathbf{r}_2 = \mathbf{r}_a$ at the location of a trapped atom, and evaluate the single-atom total decay rate $\Gamma^{(1)}_{\rm tot}(\nu_a) = \Gamma(\mathbf{r}_a, \mathbf{r}_a, \nu_a)$ and excited state level shift $J^{(1)}(\nu_a) = J(\mathbf{r}_a, \mathbf{r}_a, \nu_a)$. Figure SM3(a) shows the calculation for $\mathbf{r}_a = (0, 0, z_1)$ nm at the center of the trap shown in Fig. 1(b) of [1]. Here the total decay rate $\Gamma^{(1)}_{\rm tot} = \Gamma_{\rm 1D} + \Gamma'$ (black curve) includes the contribution from the GM of interest ($\Gamma_{\rm 1D}$), which strongly depends on the atomic resonant frequency $\nu_a = \omega_a/2\pi$ and position r_a, as well as the coupling rate to all other modes (Γ'). Γ' can be estimated from $\Gamma^{(1)}_{\rm tot}(\nu_a)$ inside the band gap ($\nu_a \gtrsim \nu_{\rm BE}$); $\Gamma'/\Gamma_0 \approx 1.1$ remains constant over a broad frequency range. Coupling rate to the TE-like GM, $\Gamma_{\rm 1D} = \Gamma^{(1)}_{\rm tot} - \Gamma'$, can be obtained from this analysis with $\Gamma_{\rm 1D}/\Gamma_0 = 1.2$.

In Fig. SM3 (a), we calculate a small excited state level shift $|J^{(1)}|/\Gamma_0 < 0.4$ over a frequency range around $\nu_1 = 335$ THz. For our experimental configuration, with $\nu_a \approx \nu_1$, we find $|J^{(1)}(\nu_a)|/\Gamma_0 \sim 0$. This also suggests that the collective level shift for two trapped atoms, $|H_{\rm dd}(x)| \equiv |J(\mathbf{r}_a, \mathbf{r}_a + x\hat{\mathbf{x}})| \ll (\Gamma_0, \Gamma_{\rm 1D})$, is negligible, where x is the atomic separation. Indeed, we do not see clear evidence of N-dependent level shifts in the steady-state transmission spectra shown in Fig. 4(a) of [1].

Figure SM3 (b) shows $\Gamma_{\rm dd}(x) \equiv |\Gamma(\mathbf{r}_a, \mathbf{r}_a + x\hat{\mathbf{x}})|$ for two trapped atoms located at the center of unit cells ($x/a \in \mathbb{Z}$) and with resonant frequencies at $\nu_a = \nu_1$ or $\nu_a > \nu_{\rm BE}$ inside the band gap, where $\Gamma^{(1)}_{\rm tot} - \Gamma' \sim 0$. For $|x| > a$, $\Gamma_{\rm dd}(x)$ can be used to estimate the dissipative coupling rate between two atoms. When $\nu_a = \nu_1$ and $|x|/a > 2$, $\Gamma_{\rm dd}(x)$ slowly drops from $\Gamma_{\rm dd}(0) - \Gamma' = 1.2\,\Gamma_0$ to smaller values as $|x|$ becomes comparable to the size of the APCW (black circles). This is caused by interference with reflections from the tapering regions surrounding the APCW. Solid line in Fig. SM3(b) shows an analytical calculation $\Gamma_{\rm dd}(x) = (\Gamma_{\rm dd}(0) - \Gamma')\cos(\pi|x|/N_{\rm eff}a)$ that compares to the numerical result, where the fitted effective number of cells $N_{\rm eff} = 162 \pm 9$ is larger than $N_{\rm cell}$ due to the leakage of the fields into the taper regions. Small variations between the analytical and numerical calculations are due to residual coupling via other channels. On the other hand, when $\nu_a > \nu_{\rm BE}$ inside the band gap, $\Gamma_{\rm dd}(x)$ quickly drops below $0.1\Gamma_0$ at $|x|/a > 2$. This is expected because, inside the band gap, atoms can only cooperatively decay via photonic channels that contribute to Γ', which are either weakly-coupled or are lost quickly into freepace within distances $|x| < 2a$.

III. LIFETIME OF TRAPPED ATOMS ALONG THE APCW

Here, we describe the lifetime measurements of trapped atoms by using the SI dipole trapping beams. The SI beam is 220 GHz red-detuned with respect to the D_2 line and has a total power of 50 mW for all measurements reported. To characterize the lifetime of trapped atoms near the APCW, we measure the normalized transmission T/T_0 as a function of the measurement time $t_{\rm m}$, as shown in Fig. 2 [1] and replotted in Fig. SM4. To ensure small population in the excited state, we choose a probe intensity well below the saturation intensity ($I/I_{\rm sat} < 0.1$) for all of our measurements, including the decay rate measurements in Section IV B. During the lifetime measurement, the frequency ν_a of the D_1 transition for the probe field $E_{\rm in}$ is located between the first and second taper resonances, which leads to the dispersive spectrum shown in Fig SM4 (a). In order to estimate the

lifetime of the trap with off resonant cavity, we employ the steady state equation [8],

$$T/T_0 = (1+\theta^2)/\left[\left(1+\frac{2C(t_{\rm m})}{1+\delta_{\rm m}^2}\right)^2+\left(\theta-\frac{2C(t_{\rm m})\delta_{\rm m}}{1+\delta_{\rm m}^2}\right)^2\right], \tag{9}$$

where the normalized detuning from the light shifted resonance Δ_0 is $\delta_{\rm m} = \frac{\Delta-\Delta_0}{\Gamma}$, the cooperativity parameter is $C(t_{\rm m}) = C_0\exp(-t_{\rm m}/\tau_{\rm GM})$ with peak cooperatively C_0, lifetime $\tau_{\rm GM}$, and normalized detuning from taper resonance θ. First, we fit the measured spectrum at $t_{\rm m} = 2.5$ ms to Eq. (9) and obtain the fitted parameters, $\theta = -0.6\pm0.1$, $C_0 = 0.24\pm0.1$, $\Gamma = 8.2\pm0.6$ MHz and $\Delta_0 = 9.3\pm0.3$ MHz as shown in black curve in Fig. SM4 (a). Then, to estimate the lifetime $\tau_{\rm GM}$, the measured data for $\Delta = 10.5$ MHz in Fig. SM4 (b) are fitted to Eq. (9) with fitted parameters from Fig. SM4 (a). We obtain the lifetime of $\tau_{\rm GM} = 28\pm2$ ms shown in black curve in Fig. SM4 (b). $\tau_{\rm GM}$ is consistently shorter than $\tau_{\rm fs}$ from free-space imaging, which might be attributed to increased heating from the stronger light intensity near the APCW, the effect of surface potentials, or outgassing from the silicon chip and structures that support the APCW. These contributions are being investigated in more detail.

IV. MODEL FOR SUPERRADIANCE OF TRAPPED ATOMS

A. A Simple Model

Here we provide a simple model that explains the the scaling of the superradiant emission observed in our experiment, and in particular the principal features of Fig. 3 in our manuscript [1]. First of all we address the role of atom number fluctuations. Consider the "textbook" case of a fixed number of atoms $N = 1, 2, 3, \cdots$, all with identical coupling. In this case, the total emission rate under weak excitation conditions as in our experiment would be $\Gamma_{\rm tot}(N) = (N-1)\Gamma_{\rm 1D} + \Gamma_{\rm tot}^{(1)}$, where $\Gamma_{\rm tot}^{(1)} = \Gamma_{\rm 1D} + \Gamma'$ is the single-atom decay rate. Clearly, superradiance only occurs for atom number greater than unity, as reflected by the superradiant rate $\Gamma_{\rm SR}(N) = (N-1)\Gamma_{\rm 1D}$, applicable only for N greater than one (i.e., superradiance requires at least two atoms).

In our experiment, the atom number N is random from trial to trial with $N = 0, 1, 2, 3, \cdots$. We take the *unconditional* distribution of atom number to be Poisson with mean $\bar{N}$. Note that because the background level in our experiment is sufficiently small as shown in Fig. SM5, any count registered heralds the presence of one or more atoms to a good approximation. Hence, in the presence of atom number fluctuations, we require the *conditional* distribution $P_1(N,\bar{N})$ that gives the probability of N atoms with $N \geqslant 1$. For a Poisson distribution of mean $\bar{N}$, the probability distribution $P_1(N,\bar{N})$ for $N \geqslant 1$ is straightforward to derive. Averaging $\Gamma_{\rm SR}(N)$ with respect to $P_1(N,\bar{N})$, we find that $\Gamma_{\rm SR}(N) \to \bar{\Gamma}_{\rm SR} = \left(\frac{\bar{N}}{1-e^{-\bar{N}}}-1\right)\Gamma_{\rm 1D}$. As expected, for $\bar{N} \gg 1$, $\Gamma_{\rm SR}(N) \to \bar{\Gamma}_{\rm SR} = \left(\bar{N}-1\right)\Gamma_{\rm 1D} \approx \bar{N}\Gamma_{\rm 1D}$. However, for $\bar{N} \to 0$, we have that $\bar{\Gamma}_{\rm SR} \to \frac{\bar{N}}{2}\Gamma_{\rm 1D}$, which expresses a small superradiant enhancement in the total decay rate for the rare trials when a second atom is present, namely $\bar{\Gamma}_{\rm tot} = \frac{\bar{N}}{2}\Gamma_{\rm 1D} + \Gamma_{\rm tot}^{(1)}$. The transition from $\bar{\Gamma}_{\rm SR} \approx \bar{N}\Gamma_{\rm 1D}$ for $\bar{N} \gg 1$ to $\bar{\Gamma}_{\rm SR} \approx \frac{\bar{N}}{2}\Gamma_{\rm 1D}$ for $\bar{N} \to 0$ in the intermediate regime for $\bar{N}$ is discussed in the quantitative analysis in the Section IV B.

In addition to taking into account the random atom number, we must also consider the sharply peaked excitation ($\propto \cos^2(kx)$) and emission ($\propto \cos^2(kx)$) couplings along the APCW, as illustrated by the inset for $\Gamma_{1D}(x)$ in Fig. 1(a) of our manuscript [1]. These two effects of excitation and emission result in an overall coupling that goes as $\zeta(x) = \cos^4(kx)$ along the APCW. Averaging over a unit cell along x gives $\langle\zeta(x)\rangle = 3/8$, since atoms are randomly distributed in the unit cell with uniform probability density due to our uniform trap configuration along x of the APCW. Because the coupling is sharply peaked, we could consider a simple model that replaces the exact form with coupling of strength unity over $3/8$ of the unit cell and zero coupling elsewhere. Roughly speaking then, randomly placed atoms over the entire unit cell would have an effective density reduced by a factor of $3/8$ relative to the case of constant coupling for all x, which is implicit in the above treatment of atom number fluctuations. We could then consider as a rough estimate that the mean number $\bar{N}$ should be rescaled to incorporate the reduced interval of coupling over the unit cell, namely $\bar{N} \to (3/8)\times\bar{N}$. That is, the value $\eta = 1$ in our simple model should be rescaled to become $\eta_{\rm simple} = 3/8$.

Overall, a simple model that incorporates both the random atom number and spatial variation of the coupling strength leads to the prediction that $\bar{\Gamma}_{\rm SR} \simeq \left(\frac{\bar{N}\eta_{\rm simple}}{1-e^{-\bar{N}\eta_{\rm simple}}}-1\right)\Gamma_{\rm 1D}$ and $\bar{\Gamma}_{\rm SR} \sim \eta_{\rm simple}\bar{N}\Gamma_{\rm 1D}$ for $\bar{N} \gg 1$, which is in reasonable accord with the results shown in Fig. (3b) of Ref. [1]. In the intermediate regime with $\bar{N} \sim 1$, the behavior is more complex, as discussed in the following section.

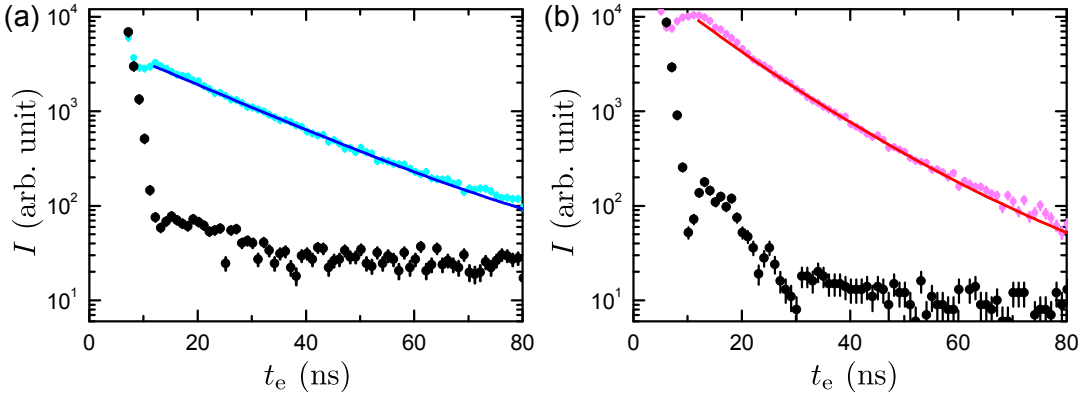

FIG. SM5: (a) Temporal profiles of backward atomic emission into the GM at $t_m = 63$ ms with and without atoms, shown in cyan and black circles, respectively. The blue curve shows Eq. (12) fitted for a single atom with $\Gamma_{1D}/\Gamma' = 1.0 \pm 0.1$. (b) Temporal profiles of atomic emission into the GM at $t_m = 3$ ms with and without atoms, shown in pink and black circles, respectively. The red curve shows Eq. (13) fitted to yield with $\bar{N} = 2.6 \pm 0.3$. The background level of (a) is higher than (b) due to the drift of the intensity modulator during the 5 times longer data accumulation time.

B. A Quantitative Analysis

The simple description in the previous section offers a qualitative understanding of superradiance for a small number of fluctuating atoms with spatially varying coupling strength. In this section, we present a quantitative analysis that takes into account our actual measurement protocol and more details of the structure and atom field coupling.

Our model of superradiance of trapped atoms is obtained by including transfer matrices for atoms in the device model described in Section I [3, 9–11]. Since the first resonance of the taper reflections is aligned to the D_1 transition for the probe E_{in}, the wavevector of the probe mode is $k = \left(1 - \frac{1}{N_{eff}}\right)\frac{\pi}{a}$ with number of cells N_{eff}, and the probe field inside the unit cell forms a nearly perfect standing wave. In addition, atoms are trapped near the central region of the APCW along the x axis ($\Delta x = \pm 10$ μm). Thus, we ignore the dephasing between atoms and envelope from the taper reflections due to the small mismatch of the wavevector $\Delta k = \frac{1}{N_{eff}}\frac{\pi}{a}$ relative to $k_0 = \frac{\pi}{a}$ at the band edge. In the following, we set the wavevector $k = k_0 = \frac{\pi}{a}$ and will discuss effects due to the Δk mismatch later. Since the overall efficiency at the transmission is lower than the one at the reflection by a factor of ~ 4, mainly due to the larger loss at the waveguide-to-fiber coupling, we use the backward atomic emission to extract the decay rate in the analysis. Note that we have confirmed that both forward and backward emission exhibit the same enhanced decay rate.

The reflection of N atoms randomly distributed at the location x_i with the coupling rate $\Gamma_{1D}\cos^2(kx_i)$ is given by,

$$r_N(\delta) = \frac{i\xi_N}{1 - i\xi_N} \quad \text{where} \quad \xi_N = -\frac{\xi_0}{i + \delta}\sum_i \cos^2(kx_i)\,. \tag{10}$$

where the single-atom fractional coupling rate is $\xi_0 = \Gamma_{1D}/\Gamma'$ and normalized detuning is $\delta = 2\Delta/\Gamma'$ with $\Gamma'/\Gamma_0 \approx 1.1$ from the numerical simulation in Section II [4]. The temporal profile of superradiance from N atoms is obtained by Fourier transforming $r_N(\delta)$ to yield $r_N(t)$, and taking the convolution of $r_N(t)$ with a gaussian pulse of the half width $\sigma \sim 5$ ns for the excitation pulse $E_{in}(t)$. Furthermore, the temporal profile at $t > 2\sigma$ can be approximated by

$$I_{r_N^{conv}}(t) = |r_N^{conv}(t)|^2 \propto \left(\Gamma_{1D}\sum_i \cos^2(kx_i)\right)^2 \cdot \exp\left[-\left(\sum_i \Gamma_{1D}\cos^2(kx_i) + \Gamma'\right)t\right]. \tag{11}$$

Considering the assumed random locations of atoms with uniform probability density in the unit cells along x, the spatially averaged temporal profile is obtained by integrating Eq. (11) along x, yielding

$$\mathcal{I}_N(t) = \gamma^2 e^{-(N\gamma+\Gamma')t}\cdot I_0(\gamma t)^{N-2}\cdot\left[\frac{N(N+1)}{4}I_0(\gamma t)^2 - \left(\frac{N}{4\gamma t} + \frac{N^2}{2}\right)I_0(\gamma t)\,I_1(\gamma t) + \frac{N(N-1)}{4}I_1(\gamma t)^2\right], \tag{12}$$

where $I_k(z)$ is a modified Bessel function of the first kind and $\gamma = \Gamma_{1D}/2$. In addition, the number of trapped atoms along the APCW is drawn from a Poisson distribution $p(\bar{N}, N)$ with mean number of atoms $\bar{N}$. The total decay curve then becomes

$$\mathcal{I}_{tot}(t) = c_0\sum_N p(\bar{N}, N)\cdot\mathcal{I}_N(t) + \mathcal{I}_{BG}, \tag{13}$$

where c_0 is a constant. Here, the background intensity $\mathcal{I}_{\rm BG}$ is measured separately without atoms and is given by the black circles in Fig. SM5. We consider decay curves of GM emission at 15 ns $< t_{\rm e} <$ 70 ns after the center of the excitation pulse shown in Fig. SM5 (i.e., after the excitation pulse is sufficiently extinguished, $t_{\rm e} >$ 15 ns, and while the background counts are negligible compared to the atomic emission, $t_{\rm e} \lesssim$ 70 ns). As shown in Fig. 3 [1], the total decay rate asymptotes to $\bar{\Gamma}^{(1)}_{\rm tot}/\Gamma_0 = 2.0 \pm 0.1$ at the longer hold times, which suggests that atomic decay at $t_{\rm m} = 63$ ms mostly originates from a single atom for mean atom number $\bar{N} \ll 1$. Note that the deviation from the exponential fit at $t_{\rm e} \gtrsim 60$ ns in the inset of Fig. 3(a) [1] is due to the spatially varying coupling rate $\Gamma_{\rm 1D}\cos^2(kx)$, which is captured by the transfer matrix model. Thus, we fit the decay curve at $t_{\rm m} = 63$ ms to Eq. (12) with $N = 1$, and obtain $\xi_0 = \Gamma_{\rm 1D}/\Gamma' = 1.0 \pm 0.1$ shown in Fig. SM5 (a). Then, by using the fitted ξ_0, the shortest hold time data ($t_{\rm m} = 3$ ms) is reasonably well fitted to Eq. (13) with $\bar{N} = 2.6 \pm 0.3$, as shown in Fig. SM5 (b). Note that the fitted $\bar{N}$ at $t_{\rm m} = 63$ ms is larger than those at shorter holding time despite the smaller $\bar{\Gamma}_{\rm tot}$, since the flux of the atomic fluorescence is higher at $t_{\rm m} = 63$ ms due to the improved overall efficiency of the device caused by $\sim 10\%$ stronger GM heating beam for cleaning the device during the longer data accumulation. The details of the systematic uncertainty for the overall efficiency are being investigated.

We also numerically estimate the contribution of the envelope from the taper reflections and dephasing between atoms along the APCW. We employ the transfer matrix model with $k = k_0 - \Delta k$, which includes the coupling rate $\Gamma_{\rm 1D}(x) \simeq \Gamma^{(0)}_{\rm 1D}\cos^2(k_0 x)\cos^2(\Delta k x)$ along the x-axis of the APCW and propagation phase $\Delta k \cdot \delta x$ between atoms separated by δx. Here, $\Gamma^{(0)}_{\rm 1D}$ denotes the peak coupling rate of both the unit cell and the envelope from taper reflections. The position of the atoms is generated from a normal distribution with $\sigma_x = 10$ μm at the temperate of 50μK. Then, we numerically generate the decay curve and extract the total decay rate, suggesting that $\Gamma_{\rm 1D}$ extracted from Eq. (12) with $N = 1$ is underestimated by $\sim 10\%$ and $\bar{N}$ from the fits to Eq. (13) by $\sim 15\%$. Note that we do not incorporate these corrections in our estimation of $\Gamma_{\rm 1D}$ and $\bar{N}$ in Ref. [1], since the temperature of the atoms trapped along the APCW could be different from the measured temperature in free space. Indeed, the calculated trap potential combined with Casimir-Polder potential suggests that atoms trapped along the APCW could be much colder ($\lesssim 20$ μK) than the measured temperature for the free-space FORT (~ 50 μK) due to the smaller trap depth near the APCW, leading to a smaller correction of $\Gamma_{\rm 1D}$ and $\bar{N}$ due to tighter localization of the atoms around the center of the APCW. The distribution of atoms along the APCW is being investigated in more detail.

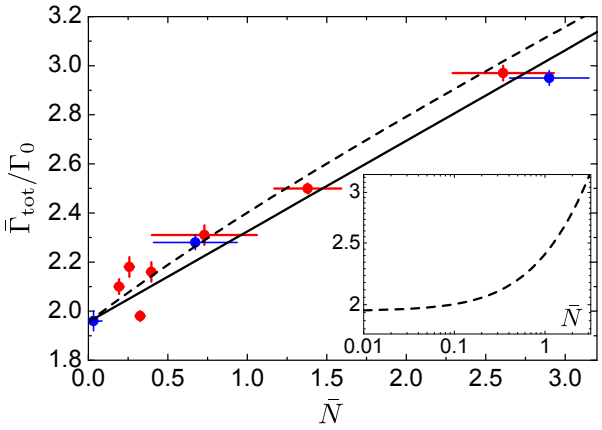

FIG. SM6: Fitted total decay rate $\bar{\Gamma}_{\rm tot}$ normalized by Γ_0 as a function of the mean number of trapped atoms $\bar{N}$. The dashed curve shows the calculated $\bar{\Gamma}_{\rm tot}$ from the model, overlaid with results measured for various hold times (red circles) and for loading times (blue circles). A linear fit to the combined data (solid black line) gives $\bar{\Gamma}_{\rm SR} = \eta \cdot \bar{N} \cdot \Gamma_{\rm 1D}$ with $\eta = 0.34 \pm 0.06$. The inset shows a log-log plot of the curve generated from the model.

To support our assumption of $\bar{N}$-dependent superradiance, $\bar{\Gamma}_{\rm tot} = \bar{\Gamma}_{\rm SR} + \bar{\Gamma}_{\rm 1D}$ with $\bar{\Gamma}_{\rm SR} = \eta \cdot \bar{N} \cdot \Gamma_{\rm 1D}$, we generate the decay curve from Eq. (13) with $\Gamma_{\rm 1D}/\Gamma_0 = 1.0$ and various $\bar{N}$, and extract $\bar{\Gamma}_{\rm tot}$ by fitting to an exponential. The dashed curve in Fig. SM6 shows the calculated $\bar{\Gamma}_{\rm tot}$, overlaid with measured hold time (red circles) and loading time (blue circles) dependence and the linear fit (solid black line). Although the dashed curve generated from the model deviates from the linear dependence at $\bar{N} < 1$, the linear fit captures the $\bar{N}$ dependence reasonably well. As clearly seen in the inset of Fig. SM6, the nonlinear dependence on $\bar{N}$ at $\bar{N} \ll 1$ is due to the "conditional" character of decay rate measurements, meaning that the decay curve consists mostly of fluorescence from a single atom, despite $\bar{N} \ll 1$. Due to the negligible background counts in our measurements, single detection events at $\bar{N} \ll 1$ herald the presence of single atoms.

The linear fit to the combined data sets gives $\bar{\Gamma}_{\rm SR} = \eta \cdot \bar{N} \cdot \Gamma_{\rm 1D}$ with $\eta = 0.34 \pm 0.06$, consistent with the model for $\bar{N} \gtrsim 0.7$. A qualitative understanding of this value of η is the following. Due to the random distribution of atoms along the APCW, the intensity of atomic emission into the GM is spatially modulated by $\cos^4(kx)$ as shown in Eq. (11), meaning that both GM excitation of atoms and emission into the GM are proportional to $\cos^2(kx)$, resulting in $\cos^4(kx)$ dependence. With the spatial

averaging along the x-axis of the APCW, the superradiant decay rate is then reduced by a factor of roughly $\eta \sim 3/8$ (i.e., the average of $\cos^4(kx)$ over a unit cell).

---

[1] A. Goban†, C. -L. Hung†, J. D. Hood†, S. -P. Yu†, J. A. Muniz, O. Painter, and H. J. Kimble, *submitted to Phys. Rev. Lett.* (2015).
[2] S.-P. Yu, J. D. Hood, J. A. Muniz, M. J. Martin, R. Norte, C.-L. Hung, S. M. Meenehan, J. D. Cohen, O. Painter, and H. J. Kimble, *Appl. Phys. Lett.* **104**, 111103 (2014).
[3] J. D. Hood *et al. in preparation* (2015).
[4] C.-L. Hung, S. M. Meenehan, D. E. Chang, O. Painter and H. J. Kimble, *New J. Phys.* **15**, 083026 (2013).
[5] G. S. Agarwal, *Phys. Rev. A* **12** 1475 (1975).
[6] S. Y. Buhmann, L. Knöll, D.-G. Welsch and H. T. Dung, *Phys. Rev. A* **70**, 052117 (2004).
[7] S. Y. Buhmann and D.-G. Welsch, *Phys. Rev. A* **77**, 012110 (2008).
[8] R. J. Thompson, Q. A. Turchette, O. Carnal, and H. J. Kimble, *Phys. Rev. A* **57**, 3084 (1998).
[9] I. H. Deutsch, R. J. C. Spreeuw, S. L. Rolston and W. D. Phillips, *Phys. Rev. A* **52**, 1394 (1995).
[10] D. E. Chang, A. S. Sørensen, E. A. Demler and M. D. Lukin, *Nat. Phys.* **3**, 807-812 (2007).
[11] D. E. Chang, L. Jiang, A. V. Gorshkov and H. J. Kimble, *New J. Phys.* **14** 063003 (2012).